Published in final edited form as:
Cancer Cell. 2012 February 14; 21(2): 155–167. doi:10.1016/j.ccr.2011.12.021.

AN ANIMAL MODEL OF MYC-DRIVEN MEDULLOBLASTOMA

Yanxin Pei[1], **Colin E. Moore**[1], **Jun Wang**[1], **Alok K. Tewari**[2], **Alexey Eroshkin**[3], **Yoon-Jae Cho**[4], **Hendrik Witt**[5], **Andrey Korshunov**[5], **Tracy-Ann Read**[6], **Julia L. Sun**[7], **Earlene M. Schmitt**[8], **C. Ryan Miller**[9], **Anne F. Buckley**[10], **Roger E. McLendon**[10], **Thomas F. Westbrook**[8,11], **Paul A. Northcott**[12], **Michael D. Taylor**[12], **Stefan M. Pfister**[5], **Phillip G. Febbo**[2], and **Robert J. Wechsler-Reya**[1,7,†]

[1]Tumor Development Program, Sanford-Burnham Medical Research Institute, La Jolla, CA

[2]Department of Medicine and Helen Diller Family Comprehensive Cancer Center, UCSF, San Francisco, CA

[3]Bioinformatics Shared Resource, Sanford-Burnham Medical Research Institute, La Jolla, CA

[4]Stanford University School of Medicine, Stanford, CA

[5]German Cancer Research Center and University of Heidelberg, Heidelberg, Germany

[6]Department of Neurosurgery, Emory University School of Medicine, Atlanta, GA

[7]Department of Pharmacology & Cancer Biology, Duke University Medical Center, Durham, NC

[8]Verna & Marrs McLean Department of Biochemistry & Molecular Biology, and Department of Molecular & Human Genetics, Baylor College of Medicine, Houston, TX

[9]Department of Pathology and Laboratory Medicine, UNC, Chapel Hill, NC

[10]Department of Pathology, Duke University Medical Center, Durham, NC

[11]Department of Pediatrics and Dan L. Duncan Cancer Center, Baylor College of Medicine, Houston, TX

[12]Hospital for Sick Children and University of Toronto, Toronto, Ontario, Canada

SUMMARY

Medulloblastoma (MB) is the most common malignant brain tumor in children. Patients whose tumors exhibit overexpression or amplification of the *MYC* oncogene (c-MYC) usually have an extremely poor prognosis, but there are no animal models of this subtype of the disease. Here we show that cerebellar stem cells expressing *Myc* and mutant *Trp53* (*p53*) generate aggressive tumors following orthotopic transplantation. These tumors consist of large, pleiomorphic cells and

†To whom correspondence should be addressed: Tumor Development Program, Sanford-Burnham Medical Research Institute, 10901, North Torrey Pines Road, La Jolla, CA 92037, rwreya@sanfordburnham.org.

Accession numbers
Microarray data have been deposited in the GEO public database (http://www.ncbi.nlm.nih.gov/geo/), with accession number GSE34126.

Supplemental information
Supplemental information includes 6 figures, 5 tables, Supplemental Experimental Procedures, and Human Tumor Analysis Supplement, and can be found at doi:_____.

resemble human MYC-driven MB at a molecular level. Notably, antagonists of PI3K/mTOR signaling, but not Hedgehog signaling, inhibit growth of tumor cells. These findings suggest that cerebellar stem cells can give rise to MYC-driven MB, and identify a novel model that can be used to test therapies for this devastating disease.

INTRODUCTION

MB is a highly malignant tumor of the cerebellum that occurs most frequently in children between 5 and 10 years of age (Polkinghorn and Tarbell, 2007). Current treatment for MB includes resection of the tumor followed by radiation and high-dose chemotherapy. Although this has resulted in significant increases in survival, ~1/3 of MB patients still die from their disease. Moreover, survivors often suffer severe side effects, including dramatic losses in cognitive function, endocrine disorders and increased susceptibility to secondary tumors (Palmer et al., 2007; Stavrou et al., 2001). Thus, more effective and less toxic therapies for MB are desperately needed.

Traditionally, MB has been classified based on histological characteristics. In this context, tumors with large cell-anaplastic (LCA) features are associated with a much poorer prognosis than classic or nodular/desmoplastic tumors (Eberhart and Burger, 2003; Leonard et al., 2001). Recently, several groups (Cho et al., 2010; Kool et al., 2008; Northcott et al., 2010; Remke et al., 2011; Thompson et al., 2006) have performed gene expression profiling and DNA copy number analysis of MB, and have identified at least 4 major subtypes of the disease: WNT, Sonic hedgehog (SHH), Group C and Group D. These molecular subtypes have distinct characteristics in terms of gene expression, mutational profiles, epidemiology and prognosis. Among molecular subtypes, tumors associated with WNT pathway activation have the most favorable outcome, whereas those that exhibit overexpression or amplification of MYC and lack WNT pathway activation (termed Group C (Northcott et al., 2010) or Group c1 (Cho et al., 2010), herein referred to as MYC-driven MB) have the worst prognosis. Although LCA histology can be found in all molecular subtypes of the disease, it is more common in MYC-driven tumors. Patients with MYC-driven MB are also more likely to exhibit metastatic disease at the time of diagnosis, to undergo recurrence, and to die of their disease (Northcott et al., 2010). More effective treatments for MYC-driven MB depend on a deeper understanding of the biology of the disease.

The fact that ectopic expression of MYC can cause MB cell lines to adopt an anaplastic phenotype (Stearns et al., 2006), and the fact that high MYC levels are associated with poor clinical outcome (Cho et al., 2010; Grotzer et al., 2001) suggest that MYC might play a key role in the biology of MB. But while the association between MYC and poor prognosis is well established, it remains unclear whether the gene is involved in tumor initiation, maintenance or progression. Likewise, MYC-driven tumors frequently exhibit loss of one allele of the *TP53* tumor suppressor (in context of isochromosome 17q) (Northcott et al., 2010; Pfister et al., 2009), and LCA tumors have been reported to express high levels of p53 protein, an indicator of dysregulation of the TP53 pathway (Eberhart et al., 2005; Frank et al., 2004). However, it is not clear if alterations in TP53 represent causal events.

Animal models of brain tumors can be generated by targeting expression of oncogenes to neural progenitors or stem cells. Recent studies suggest that different populations of progenitors may be susceptible to transformation by distinct signaling pathways (Gilbertson and Ellison, 2008). For example, mutations in the SHH pathway promote transformation of granule neuron precursors (GNPs) in the external germinal layer of the cerebellum (Schuller et al., 2008; Yang et al., 2008), whereas dysregulation of WNT signaling causes transformation of progenitors in the lower rhombic lip and embryonic dorsal brainstem

(Gibson et al., 2010). We recently identified a population of stem cells in the white matter of the postnatal cerebellum (Lee et al., 2005), and hypothesized that they might give rise to some types of MB. To test this hypothesis and to address the functional importance of *MYC* and *TP53* in MB, we examined the effects of overexpressing *Myc* and disrupting *p53* function in these cells.

RESULTS

Myc promotes proliferation of cerebellar stem cells *in vitro*

Stem cells can be isolated from the postnatal cerebellum based on expression of Prominin1 (CD133) and lack of neuronal and glial lineage markers ($Prom1^{+}Lin^{-}$). To investigate the effects of *Myc* on these cells, we infected them with control retroviruses or viruses encoding a stabilized form of *Myc* (Myc^{T58A}) (Chang et al., 2000) and measured their proliferation. As shown in Figure 1A, *Myc*-infected cells showed a 2.5 fold increase in proliferation compared to cells infected with control viruses. To examine the effects of *Myc* on self-renewal, infected $Prom1^{+}$ Lin^{-} cells were cultured at low density (2000 cell/ml) in the presence of basic fibroblast growth factor (bFGF) and epidermal growth factor (EGF) to promote neurosphere formation. As shown in Figures 1B–D, the number of neurospheres in *Myc*-infected cultures was 9-fold higher than that in control cultures. To determine whether the effects of *Myc* persisted in longer-term cultures, neurospheres were dissociated into single-cell suspensions and re-plated every 7 days. Over the course of 5 weeks, *Myc*-infected cultures exhibited a 1000-fold increase in cell number, compared to a 2-fold increase in control cultures (Figure S1). These data indicate that overexpression of *Myc* in cerebellar stem cells promotes short-term proliferation as well as long-term self-renewal *in vitro*.

Myc-expressing stem cells form transient hyperplastic lesions *in vivo*

In light of the above results, we investigated whether *Myc*-expressing cells could give rise to tumors *in vivo*. We stereotaxically implanted control (GFP virus-infected) or *Myc*-infected stem cells into the cerebellum of immunocompromised (NOD-SCID-IL2RGamma^{null}, or NSG) mice and examined cerebella of recipients 2–3 weeks later. As shown in Figures 2A–B, in animals that had received control cells, few infected cells (marked by GFP) could be detected, and only a small proportion of these were proliferating (based on Ki67 staining). In contrast, in animals transplanted with *Myc*-expressing cells, large masses of infected cells could be detected, and the majority of these were proliferating (Figures 2C–F). These results suggest that *Myc*-infected cells can undergo persistent proliferation *in vivo*.

To determine whether *Myc*-infected cells can continue to grow and give rise to tumors, we sacrificed animals (n=5) four weeks after transplantation. Surprisingly, at this stage, few transplanted cells could be detected in the cerebellum of mice that had received either control or *Myc* infected cells. Consistent with this, we followed a cohort of mice (n=6) transplanted with *Myc*-infected cells for 6 months, and found that none of them developed symptoms during this period (data not shown). This suggested that *Myc* can drive proliferation of stem cells, but is not sufficient to promote tumor growth.

The fact that *Myc* infected cells formed large masses 2 weeks after transplantation but were undetectable 4 weeks after transplantation raised the question of what happened to these cells. Since *Myc* can induce apoptosis as well as proliferation (Pelengaris et al., 2000) we examined cerebella from recipients of control and *Myc*-infected cells for evidence of apoptosis by staining with anti-cleaved caspase 3 (CC3). Few control virus-infected cells were labeled with anti-CC3 (although some staining was seen around the transplant site) whereas *Myc*-infected cells exhibited a significant amount of CC3 staining (Figures 2G–H),

suggesting that they were undergoing apoptosis *in situ*. These data suggest that *Myc* promotes proliferation as well as apoptosis of cerebellar stem cells.

Mutant *p53* synergizes with *Myc* to promote tumor formation

MYC-induced apoptosis is frequently dependent on *TP53* (Hermeking and Eick, 1994). To test whether inactivation of *p53* could inhibit *Myc*-induced cell death in cerebellar stem cells, we measured apoptosis in cells infected with control (GFP), *Myc*, *DNp53* (Bowman et al., 1996) or *Myc* + *DNp53* viruses. As shown in Figure S2A–D, cells infected with *Myc* viruses alone exhibited a marked increase in apoptosis compared to cells infected with control viruses (Figures S2A–B), but *DNp53* completely abolished the pro-apoptotic effects of *Myc* (Figures S2C–D). These results suggest that *Myc* mediated apoptosis of stem cells can be blocked by inhibition of *p53* function.

The above findings raised the possibility that cells overexpressing *Myc* and *DNp53* might be able to give rise to tumors. To test this, we co-infected stem cells with viruses encoding these genes and implanted them into the cerebellum of NSG mice. Animals transplanted with cells co-expressing the two genes developed highly aggressive tumors and had to be sacrificed between 6–12 weeks (Figures 3A–B). These experiments were performed using the T58A mutant of *Myc*. Notably, stem cells infected with WT *Myc* + *DNp53* also gave rise to tumors, albeit with reduced penetrance (33%) and longer latency (15–20 weeks). These studies suggest that mutant *p53* can cooperate with *Myc* to promote transformation of cerebellar stem cells.

We characterized tumors arising from stem cells infected with *Myc* and *DNp53* (MP tumors) using tumors from *Ptch1* mutant mice (a model for SHH-associated MB) for comparison (Figures 3C–H). Whereas $Ptch1^{+/-}$ tumor cells were not much bigger than normal granule neurons (~ 5 μm, compare arrow to arrowhead in Figure 3H), cells from MP tumors were approximately 5 times bigger (~ 25 μm, compare vertical and horizontal arrows in Figure 3E). In addition, MP tumors exhibited prominent necrosis (asterisk in Figure 3C) and nuclear molding (arrows in Figures 3D–E), whereas $Ptch1^{+/-}$ tumors rarely displayed these features (Figures 3G–H). Importantly, the histological features of murine MP tumors resembled those of human LCA (Group C) MB (Figure S3). Together these data suggested that MP tumors are distinct from SHH-driven tumors and histologically resemble human LCA MB.

Immunohistochemical characterization of MP tumors demonstrated that they have a high proliferative index and often express the stem cell/progenitor marker Nestin (Figures 4A–4C). Tumor cells that did exhibit differentiation predominantly expressed the early neuronal lineage marker Tuj1 (class III beta-tubulin, Figure 4D). Only rare tumor cells expressed the mature neuronal marker synaptophysin (not shown) or the astrocytic marker GFAP (Figure 4E), consistent with the notion that MP tumors are poorly differentiated. Tumors also did not express O4, NG2, PDGFRa or SOX10, markers associated with oligodendrogliomas (data not shown). Finally, tumor cells expressed significant amounts of the chromatin remodeling protein BAF47 (also known as Smarcb1, Snf5 or Ini1), which is commonly lost in atypical teratoid/rhabdoid tumor (AT/RT), suggesting that we were not modeling this type of tumor (Figure 4F). Based on these observations, we concluded that MP tumors are highly proliferative and poorly differentiated, features consistent with LCA MB.

MP tumors can be generated from granule neuron precursors

Previous studies have suggested that SHH-associated MB can be initiated in GNPs or neural stem cells (Schuller et al., 2008; Yang et al., 2008), We therefore determined whether GNPs could also be transformed by *Myc* and *DNp53*. To test this, we FACS-sorted GFP^+ cells

(GNPs) from neonatal Math1-GFP transgenic mice (Lee et al., 2005; Lumpkin et al., 2003) (Figures S4A, B), infected these cells with *Myc* and *DNp53* viruses, and then transplanted them into the cerebellum of NSG mice. We found that 7 out of 22 recipients developed tumors, with a latency of 108 days (Figure S4D, E, F). Interestingly, although the cells were GFP^+ prior to transplantation (Figure S4B), the tumors that developed from them were no longer GFP^+ when analyzed by microscopy or flow cytometry (Figures S4C, E), suggesting that they had lost a key marker of the granule lineage during the course of transformation. These studies demonstrate that both stem cells and GNPs can give rise to MYC-driven tumors.

Myc is required to maintain MP tumor growth

In many tumors driven by MYC, shutting off the expression of MYC results in tumor regression (Jain et al., 2002; Soucek et al., 2008). To determine whether MP tumors continue to depend on *Myc* once they are established, we infected stem cells with viruses encoding a tetracycline–inducible form of *Myc* along with *DNp53*-IRES-Luciferase, and transplanted these cells into the cerebellum of NSG mice. Mice were fed doxycycline (DOX)-containing food until they developed tumors (3–4 weeks after transplantation). Tumors were removed, dissociated and re-transplanted into cerebella of naïve NSG mice. Secondary recipients were separated into 3 groups: Group 1 (n=14) was maintained on DOX-containing food; Group 2 (n=14) was fed DOX-containing food for 1 week, then switched to normal food; and Group 3 (n=12) was fed food without DOX (Figure 5A). Animals in all groups developed bioluminescent signals (from the luciferase encoded by the *DNp53* virus), indicating the presence of transplanted tumor cells. Group 1 animals showed a rapid and dramatic increase in bioluminescence (Figure 5B, top graph), and by 3–4 weeks after transplantation, all mice had developed symptoms and had to be sacrificed (Figure 5F). Analysis of brains from these mice revealed large tumors in every animal (Figure 5C). In contrast, bioluminescence in Group 2 and 3 mice decayed in the absence of DOX (Figure 5B, bottom two graphs). Moreover, no tumors could be detected in these animals 3 weeks after transplantation (Figures 5D–E), and animals remained asymptomatic at 6 weeks (Figure 5F). Together these data suggest that *Myc* is not only necessary for tumor initiation but is also required to maintain growth of MP tumors.

MP tumors resemble human MYC-driven MB

Our histological analysis indicated that MP tumors resemble human LCA MB. Since LCA histology is more common in MYC-driven tumors (Cho et al., 2010; Northcott et al., 2010), this supported the notion that MP tumors might represent a model for human MYC-driven MB. To test whether MP tumors resembled human MYC-driven MB at a molecular level, we performed gene expression analysis of MP tumors and compared the resulting gene expression profiles with profiles of the 4 subtypes of human MB (WNT, SHH, Group C and Group D) defined by (Northcott et al., 2010). In this classification scheme, Group C tumors, which are associated with the poorest prognosis, frequently exhibit amplification or overexpression of MYC (Northcott et al., 2010). Using genes differentially expressed in each subgroup and previously published methods (Bild et al., 2006), we identified 4 sets of genes (“subgroup signatures”) whose expression accurately predicted the subgroup of the human MB samples (see Human Tumor Analysis Supplement).

Human MB subgroup signatures were then applied to gene expression data from murine MP and *Ptch1* mutant tumors, with each tumor receiving a subgroup signature score representing its similarity to each subgroup of human MB. As shown in Figure 6A and Table S1, murine *Ptch1* tumors most closely resembled human SHH associated tumors, with one exception, which possessed a profile consistent with both the WNT and SHH groups. In contrast, MP tumors were most similar to Group C/D tumors, with the exception of a tumor that

resembled both the WNT and Group C/D signatures. To validate these findings, we compared data from murine tumors to expression profiles from a distinct set of human MB samples (Cho et al., 2010). Utilizing a subclass mapping algorithm (Hoshida et al., 2007) we generated a similarity metric between MP tumors and the MB subgroups defined in Cho et al. As shown in Figure S5, this analysis revealed a high degree of similarity between MP tumors and the 'c1' subtype of human MB, which is characterized by copy number gains of c-MYC and gene expression signatures indicative of robust MYC transcriptional activity (Cho et al. 2010).

Finally, we stained an independent set of MP and *Ptch1* tumors with antibodies that have been found to mark each of the 4 human MB subgroups (Northcott et al., 2010). Murine *Ptch1* mutant tumors expressed high levels of the SHH subgroup marker SFRP1 (Figure 6B) and lacked expression of the WNT subgroup marker nuclear CTNNB1 (not shown), the Group C marker NPR3 (Figure 6C) and the Group D marker KCNA1 (Figure 6D). In contrast, MP tumors exhibited high levels of NPR3 (Figure 6F) and lacked expression of the other markers (Figures 6E, G and data not shown). Together, these data suggested that MP tumors resemble human Group C (MYC-driven) MB.

Gene expression profile of MP tumors

We compared the gene expression profiles of MP tumors to those of freshly isolated cerebellar stem cells and tumors from *Ptch1* mutant mice. Using principal component analysis – an unsupervised approach designed to group samples based on their similarity in gene expression – we determined that MP tumors generated by infection of $Prom1^{+}Lin^{-}$ stem cells and those generated by infection of $Prom1^{+}$ cells were indistinguishable based upon global RNA expression (Figure 7A). Both of these tumor types were distinct from normal (uninfected) cerebellar stem cells and from *Ptch1* mutant tumors. Hierarchical clustering (Figure 7B) confirmed the similarity between MP tumors generated from $Prom1^{+}Lin^{-}$ and $Prom1^{+}$ cells as well as the differences between these tumors, *Ptch1* tumors and normal stem cells. Focusing on changes in gene expression of 3-fold and higher (p-value with FDR correction < 0.0001), we identified 1228 genes (1465 probe sets) that were differentially expressed between MP tumors and *Ptch1* tumors (Table S2), and 812 genes (955 probe sets) differentially expressed between MP tumors and normal stem cells (Table S3).

To learn about the functional significance of these genes, we analyzed them using Gene Set Enrichment Analysis (GSEA) (Subramanian et al., 2005) and using NextBio software (Kupershmidt et al., 2010) (see Figure 7 and Tables S4–S5). Several important correlations emerged from this analysis. First, we noted that genes expressed at high levels in MP tumors were similar to those found to be targets of MYC in other studies (Figure 7C, Tables S4–S5). Another set of differentially expressed genes, which exhibited decreased expression in MP tumors, were targets of forkhead transcription factors (e.g. *Foxo1*, Figure 7D). This is notable because FOXO proteins often inhibit expression of MYC targets, induce expression of MYC antagonists, and suppress MYC-induced transformation (Bouchard et al., 2007; Bouchard et al., 2004; Delpuech et al., 2007). We also noted a marked similarity between genes expressed in MP tumors and those enriched in embryonic stem (ES) cells and induced pluripotent stem (iPS) cells, including those induced by *Oct4* and *Klf4* (i.e., in the absence of exogenous *Myc*) (Figure 7F). These genes were enriched in MP tumors compared to *Ptch1* tumors, consistent with the fact that the former are derived from stem cells and the latter originate from lineage-restricted neuronal progenitors. However, they were also enriched in MP tumors compared to cerebellar stem cells, suggesting that MP tumors have adopted a more primitive differentiation state than the cells from which they were derived. In support of this notion, MP tumors showed decreased expression of genes associated with neuronal lineage commitment and differentiation (Figure 7E). Finally, our analysis revealed

significant enrichment of a PI3K signaling gene set as well as a set of genes down-regulated by rapamycin in another cancer cell line (Tables S4–5). Notably, analysis of human MYC-driven (Group c1) tumors using Connectivity Map (CMAP) – an algorithm that screens a given gene expression signature against a compendium of drug-induced gene expression signatures (Lamb et al., 2006) – suggested that genes regulated by PI3K and mTOR inhibitors are also enriched in these tumors (Table S6). These observations, and the fact that MP tumors have decreased expression of Foxo targets, which are negatively regulated by the PI3K pathway, suggested that this pathway might play an important role in tumor growth.

MP tumors are sensitive to inhibitors of PI3 Kinase and mTOR

To determine whether MP tumors were dependent on PI3K/mTOR signaling, we first tested the effects of PI3K/mTOR inhibitors on tumor cell growth in vitro (Figure 8A). MP tumors showed complete growth inhibition in the presence of 1–5 μM BEZ-235 (an antagonist of both PI3K and mTOR) and 5 μM BKM-120 (an antagonist of PI3K), and partial inhibition in the presence of lower concentrations of these compounds. The mTOR antagonist RAD-001 also inhibited growth, albeit incompletely, at concentrations of 0.2 – 5 μM. Consistent with their continued dependency on *Myc*, tumor cells were dramatically inhibited by 10058-F4, a small molecule that interferes with Myc-Max dimerization (Huang et al., 2006). In contrast, we found that MP tumor cells showed no growth inhibition in response to the SHH antagonist cyclopamine.

To determine whether BEZ-235 and BKM-120 could also affect long-term tumor cell growth, we cultured MP tumor cells for 3, 7 or 14 days in the presence of these inhibitors, and counted cell number at each time point. We found that all three doses of BEZ-235 inhibited cell growth whereas only the highest concentration of BKM-120 (5 μM) was able to cause growth inhibition (Figure 7B). Similar results were observed when we used neurosphere assays to measure tumor cell clonogenicity (Figure S6).

To confirm that these compounds were acting on the PI3K/mTOR pathway, we performed western blotting to analyze phosphorylation of critical proteins in the pathway. As shown in Figure 8C, MP tumor cells showed substantial amounts of phospho-AKT and phospho-S6 in the absence of inhibitors (DMSO lanes). Treatment with BEZ-235 or BKM-120 inhibited phosphorylation of both AKT and S6. In contrast, RAD-001 inhibited S6 phosphorylation but did not affect phospho-AKT. The fact that BEZ-235 and BKM-120 were more potent inhibitors of tumor cell proliferation than RAD-001 (Figures 8A–B) suggested that blocking activity of PI3K, or both PI3K and mTOR, might be required for effective tumor inhibition.

To determine whether inhibition of PI3K/mTOR signaling could also inhibit growth of MP tumors in vivo, we isolated MP tumor cells and transplanted them into naïve NSG mice. After 7 days, we began treating animals with BKM-120 once daily until clinical signs of tumor formation were observed. Animals treated with BKM-120 survived significantly longer than controls (median survival = 35 vs. 25 days) (Figure 8D). These results suggest that inhibitors of PI3K/mTOR signaling might be useful for treatment of MYC-driven MB.

DISCUSSION

MYC-driven MB is a highly malignant pediatric brain tumor that is often resistant to conventional radiation and chemotherapy. More effective approaches to treat this disease are critical, and these can be facilitated by the development of robust animal models. The fact that a subset of human MBs exhibit amplification or overexpression of MYC prompted us to develop a mouse model that can be used to investigate the biology of and test therapies for MYC-driven MB.

Cooperation between *Myc* and mutant *p53*

Our observation that *Myc* induces proliferation of cerebellar stem cells is consistent with previous reports showing mitogenic effects of *Myc* in normal and malignant stem cells (Nagao et al., 2008; Wang et al., 2008). However, while *Myc* can promote proliferation of cerebellar stem cells *in vitro*, it cannot, on its own, sustain long-term growth *in vivo*. Our studies suggest that this is due to *Myc*-induced apoptosis, but this raises the question: why are these cells more sensitive to apoptosis *in vivo*? One reason may be that *in vitro* they are maintained under conditions that favor neurosphere formation, including high levels of EGF and bFGF. In the presence of such growth factors, the proliferative response to *Myc* often dominates over the apoptotic response (Harrington et al., 1994). It is also possible that the *in vivo* microenvironment contains factors that actively inhibit growth or survival of transplanted stem cells. In either case, it is clear that the potent mitogenic effects of *Myc* are insufficient to drive transformation.

Whereas stem cells expressing *Myc* alone do not form tumors, cells expressing *Myc* and mutant *p53* are highly tumorigenic. Dysregulation of the *TP53* pathway, as evidenced by elevated expression of p53 protein, is a common feature of human LCA MB (Eberhart et al., 2005; Frank et al., 2004; Tabori et al., 2010). Moreover, human MYC-driven MBs often exhibit isochromosome 17q, which is associated with monoallelic loss of *TP53* (Cho et al., 2010; Northcott et al., 2010). Thus, loss of p53 function could synergize with MYC overexpression in human MB as well. The ability of mutant TP53 to cooperate with MYC has been observed in many other cancers (Elson et al., 1995; Hemann et al., 2005), but the mechanisms underlying this cooperation are not fully understood. In our system, *Myc*-induced apoptosis is dependent on endogenous p53, and DNp53 acts, at least in part, by blocking this function. (Hermeking and Eick, 1994). However, loss of *p53* function has also been reported to increase neural stem cell self-renewal and to promote pluripotency (Kawamura et al., 2009; Meletis et al., 2006; Zheng et al., 2008), both of which could certainly contribute to transformation. Moreover, loss of *p53* function promotes genomic instability (Hanel and Moll, 2011), which could result in additional mutations that promote tumor formation. Which of these functions of *p53* are most critical in our tumors is the subject of ongoing studies.

Our observation that stem cells can be transformed by the combination of *Myc* and *DNp53* – but not by either gene alone – suggests that these genes are both required for tumor initiation. But whether initiating oncogenes continue to be required once tumors are formed is unclear. Previous studies have demonstrated that in many types of cancer, tumors become addicted to expression of the oncogene and undergo regression when expression is shut off (Jain et al., 2002; Soucek et al., 2008). However, there have been reports of tumors that continue to grow even when *Myc* is silenced (Boxer et al., 2004). Our results suggest that continued expression of *Myc* is required for maintenance of MP tumor growth. If similar findings hold true for human MYC-driven MB, it would suggest that targeting MYC itself might be an effective approach to therapy.

MP tumors as a model for human MB

The tumors that are induced by *Myc* and *DNp53* resemble human LCA and MYC-driven MB. Interestingly, two other groups have recently described animal models of LCA MB. Deletion of *Rb* and *p53* in neural progenitors results in tumors that exhibit amplification of *MycN* and resemble LCA MB (Shakhova et al., 2006). Likewise, mice in which *MycN* is overexpressed in $Glt1^{+}$ progenitors develop either classic or LCA MB (Swartling et al., 2010). While each of these tumors exhibits large cell-anaplastic histology, it is important to note that they may not all represent the same subtype of MB. We have previously reported that LCA histology can occur in all molecular subgroups of MB, including WNT, SHH,

Group C and Group D tumors (Northcott et al., 2010). However, MBs that overexpress MYCN are largely distinct from those that overexpress MYC. Thus, the models described by these groups may correspond to human MYCN-associated MB, whereas MP tumors may represent human MYC-driven (Group C) MB. Interestingly, tumors of a recently developed MB model in which *Rb* and *p53* were deleted in postnatal cerebellar stem cells did not overexpress *MycN* and, like our tumors, expressed high levels of NSC markers (Sutter et al., 2010). It will be interesting to compare these models at a molecular level to determine the similarities and differences between them.

Cellular origins of *Myc* associated tumors

Previous studies have shown that activation of the SHH pathway in GNPs results in MB with 100% penetrance (Schuller et al., 2008; Yang et al., 2008). Moreover, activation of the SHH pathway in stem cells within the cerebellar ventricular zone (VZ) results in expansion of the VZ, but cells do not become transformed until they commit to the granule lineage (Schuller et al., 2008; Yang et al., 2008). These studies suggest that lineage restriction is a critical determinant of susceptibility to transformation by SHH signaling. The current studies suggest that *Myc* + *DNp53* can also cause transformation of both stem cells and GNPs. However, once transformed, the stem cells do not appear to undergo lineage commitment; indeed, their gene expression profile suggests that *Myc*/*DNp53*-transformed cells are even more immature or undifferentiated than normal neural stem cells. Moreover, when GNPs are infected with *Myc* and *DNp53* viruses, they lose expression of GNP lineage markers during the course of transformation. These results demonstrate that stem cells and GNPs can both serve as cells of origin for MYC-driven MB, and suggest that lineage commitment is not required for (and in fact, may be incompatible with) transformation.

Molecular phenotype of MP tumors

In addition to highlighting the similarities between MP tumors and human MYC-driven MB, our gene expression analysis also revealed that genes overexpressed in MP tumors are similar to those expressed by embryonic and pluripotent stem cells. The association between pluripotency and cancer has been noted in a number of other systems. For example, in breast cancer, glioblastoma and bladder carcinoma, an ES-like signature is associated with aggressive, poorly differentiated tumors and is a predictor of poor prognosis (Ben-Porath et al., 2008). Likewise, a pluripotency signature is associated with transformation of follicular lymphoma to diffuse large B-cell lymphoma (Gentles et al., 2009). There has been some debate about whether this signature reflects true acquisition of pluripotent characteristics or simply activation of a *MYC*-driven gene expression profile (Kim et al., 2010). In the case of MP tumors, there is no question that a *Myc*-driven transcriptional program is active and plays a significant role in driving tumor growth. However, it is worth noting that the genes identified as differentially expressed in MP tumors also resemble those associated with pluripotency induced by *Oct4* and *Klf4* suggesting that the pluripotency program in our cells is not purely a consequence of *Myc* overexpression. It is also notable that MP tumors express lower levels of neural differentiation markers compared to not only *Ptch1* tumors (which consist of neuronal progenitor-like cells) but also normal neural stem cells from which they were derived. These findings suggest that transformation of NSCs may involve de-differentiation to a more pluripotent state.

Among the most important results of our analysis was the observation that MP tumors have increased expression of genes associated with PI3K/AKT/mTOR signaling and decreased expression of *Foxo* target genes. FOXO proteins have been shown to inhibit expression of MYC targets (Bouchard et al., 2004), and MYC-induced transformation requires inactivation of FOXO proteins (Bouchard et al., 2007). Importantly, AKT has been shown to phosphorylate FOXO proteins and thereby prevent them from entering the nucleus

(Bouchard et al., 2004). Although the cause of PI3K pathway activation in MP tumors is unclear, it seems likely that this activation interferes with Foxo activity and thereby synergizes with Myc overexpression to promote transformation. PI3K signaling has also been shown to increase Myc protein stability (Kumar et al., 2006) and to enhance Myc function by promoting degradation of its antagonist Mad1 (Zhu et al., 2008). Thus, the PI3K pathway may be a critical regulator of transformation in MP tumors.

In light of the above findings, we hypothesized that inhibition of PI3K signaling might block growth of MP tumors. Whereas inhibition of the SHH pathway had little effect on growth of these cells, treatment with the PI3K/mTOR inhibitors BEZ-235 and BKM-120 had a potent inhibitory effect on tumor growth both in vitro and in vivo. Several studies have documented activation of PI3K signaling in human MB (Castellino et al., 2010; Hartmann et al., 2006). In particular, genomic analysis suggests that MYC-driven MBs frequently exhibit loss of chromosome 10q (where *PTEN* is located) (Northcott et al., 2010). Consistent with this, our CMAP analysis (Table S6) suggests that MYC-driven tumors have elevated expression of genes that are regulated by PI3K and mTOR inhibitors. Together, these findings suggest that targeting the PI3K/mTOR pathway may be useful for treatment of human MB. Further studies using this novel model of MYC-driven MB will shed light on the biology of this disease and open up new targets for therapy.

EXPERIMENTAL PROCEDURES

Animals

C57BL/6J mice used as a source of stem cells and immunocompromised (NOD-scid IL2Rgamma^{null} or NSG) mice used for transplantation were purchased from Jackson Labs (Bar Harbor, ME). Mice were maintained in the Cancer Center Isolation Facility at Duke University and in the Animal Facility at Sanford-Burnham. All experiments were performed in accordance with national guidelines and regulations, and with the approval of the animal care and use committees at each institution.

Orthotopic transplantation and tumor formation

Before transplantation, cerebellar stem cells (Prom1^{+}Lin^{-} cells) or GNPs (GFP^{+} cells FACS-sorted from Math1-GFP transgenic mice) were infected with *Myc* and *DNp53* retroviruses for 20 hr. 1×10^{5} stem cells in Neurocult medium or 1 x 10^{6} GNPs suspended in Neurobasal medium were injected into the cerebellum of NSG mice (6–8 weeks old) using a stereotaxic frame with a mouse adaptor (David Kopf Instruments), as described previously (Yang et al., 2008). Animals were monitored weekly, and sacrificed when they showed symptoms of MB.

To generate Tetracycline (Tet)-regulatable tumors, stem cells were infected with Tet-inducible *Myc* lentivirus and *DNp53* retrovirus. The Tet-inducible vector (pICUE-myc^{T58A}) consisted of a Tet-response element (TRE2) controlling expression of turbo red fluorescent protein (tRFP) and *Myc*-T58A and a constitutive promoter controlling expression of the reverse tetracycline transactivator (rtTA3) and eGFP (Meerbrey et al., 2011). Infected cells were implanted into cerebella of NSG mice, and mice were manintained on DOX-containing food. When mice became symptomatic, they were sacrificed and tumor cells were re-transplanted into secondary NSG mice. These mice were separated into three groups. Group 1 (n= 14) was continually fed DOX-containing food, Group 2 (n=14) was fed DOX-food for one week and normal food thereafter; and Group 3 (n=12) was not fed DOX-food at all. Mice were subjected to bioluminescent imaging at 1, 2 and 3 weeks, and sacrificed at onset of symptoms. At time of sacrifice, brains were removed and paraffin-embedded, sectioned and stained with H&E.

In vivo bioluminescent imaging

Mice were given intraperitoneal injections of 150 ng/g D-Luciferin (Caliper Life Sciences, cat#12279) and anesthetized with 2.5% isoflurane. 7–8 min after injection, animals were imaged using the Xenogen Spectrum (IVIS-200) imaging system.

In vivo inhibitor treatment

To study effects of the PI3-kinase antagonist BKM-120 on tumor growth *in vivo*, we re-transplanted 500 MP tumor cells into cerebella of secondary NSG mice. 7 days after transplantation, mice were randomly separated into two groups: Group 1 was given vehicle (0.5% methyl-cellulose) and Group 2 was given 30 mg/kg BKM-120 by oral gavage once daily until symptom onset. BKM-120 was dissolved in 0.5% methylcellulose and sonicated using an ultrasonicator (Misonix) at an amplitude of 20 for 12 min. Survival was defined as the time from transplantation until symptom onset.

Supplementary Material

Refer to Web version on PubMed Central for supplementary material.

Acknowledgments

We dedicate this paper to the memory of Cameron Jackson. In addition, we would like to thank Jack Dutton and Adriana Charbono for assistance with animal colony maintenance and screening, Beth Harvat, Lynn Martinek, Mike Cook, Amy Cortez and Yoav Altman for help with flow cytometry, Zhengzheng Wei for processing and analysis of microarrays, Irina Leiss for performing immunohistochemistry and Daisuke Kawauchi and Martine Roussel for helpful discussions. This work was supported by funds from the Alexander and Margaret Stewart Trust and the Duke Comprehensive Cancer Center (RWR), the Southeastern Brain Tumor Foundation (RWR), Alex's Lemonade Stand Foundation (RWR), Pediatric Brain Tumor Foundation (REM and RWR), NCI grant numbers CA122759 (RWR) and CA159859 (MDT and RWR). CRM is a Damon Runyon-Genentech Clinical Investigator supported in part by a grant (CI-45-09) from the Damon Runyon Cancer Research Foundation. RWR is supported by a Leadership Award (LA1-01747) from the California Institute of Regenerative Medicine (RWR).

Abbreviations

MB	medulloblastoma
LCA	large cell-anaplastic
SHH	sonic hedgehog
DN	dominant-negative
MP	*Myc*/*DNp53*
CC3	cleaved caspase 3

References

Ben-Porath I, Thomson MW, Carey VJ, Ge R, Bell GW, Regev A, Weinberg RA. An embryonic stem cell-like gene expression signature in poorly differentiated aggressive human tumors. Nat Genet. 2008; 40:499–507. [PubMed: 18443585]

Bild AH, Yao G, Chang JT, Wang Q, Potti A, Chasse D, Joshi MB, Harpole D, Lancaster JM, Berchuck A, et al. Oncogenic pathway signatures in human cancers as a guide to targeted therapies. Nature. 2006

Bouchard C, Lee S, Paulus-Hock V, Loddenkemper C, Eilers M, Schmitt CA. FoxO transcription factors suppress Myc-driven lymphomagenesis via direct activation of Arf. Genes Dev. 2007; 21:2775–2787. [PubMed: 17974917]

Bouchard C, Marquardt J, Bras A, Medema RH, Eilers M. Myc-induced proliferation and transformation require Akt-mediated phosphorylation of FoxO proteins. EMBO J. 2004; 23:2830–2840. [PubMed: 15241468]

Bowman T, Symonds H, Gu L, Yin C, Oren M, Van Dyke T. Tissue-specific inactivation of p53 tumor suppression in the mouse. Genes Dev. 1996; 10:826–835. [PubMed: 8846919]

Boxer RB, Jang JW, Sintasath L, Chodosh LA. Lack of sustained regression of c-MYC-induced mammary adenocarcinomas following brief or prolonged MYC inactivation. Cancer Cell. 2004; 6:577–586. [PubMed: 15607962]

Castellino RC, Barwick BG, Schniederjan M, Buss MC, Becher O, Hambardzumyan D, Macdonald TJ, Brat DJ, Durden DL. Heterozygosity for pten promotes tumorigenesis in a mouse model of medulloblastoma. PLoS One. 2010; 5:e10849. [PubMed: 20520772]

Chang DW, Claassen GF, Hann SR, Cole MD. The c-Myc transactivation domain is a direct modulator of apoptotic versus proliferative signals. Mol Cell Biol. 2000; 20:4309–4319. [PubMed: 10825194]

Cho YJ, Tsherniak A, Tamayo P, Santagata S, Ligon A, Greulich H, Berhoukim R, Amani V, Goumnerova L, Eberhart CG, et al. Integrative Genomic Analysis of Medulloblastoma Identifies a Molecular Subgroup That Drives Poor Clinical Outcome. J Clin Oncol. 2010

Delpuech O, Griffiths B, East P, Essafi A, Lam EW, Burgering B, Downward J, Schulze A. Induction of Mxi1-SR alpha by FOXO3a contributes to repression of Myc-dependent gene expression. Mol Cell Biol. 2007; 27:4917–4930. [PubMed: 17452451]

Eberhart CG, Burger PC. Anaplasia and grading in medulloblastomas. Brain Pathol. 2003; 13:376–385. [PubMed: 12946027]

Eberhart CG, Chaudhry A, Daniel RW, Khaki L, Shah KV, Gravitt PE. Increased p53 immunopositivity in anaplastic medulloblastoma and supratentorial PNET is not caused by JC virus. BMC Cancer. 2005; 5:19. [PubMed: 15717928]

Elson A, Deng C, Campos-Torres J, Donehower LA, Leder P. The MMTV/c-myc transgene and p53 null alleles collaborate to induce T-cell lymphomas, but not mammary carcinomas in transgenic mice. Oncogene. 1995; 11:181–190. [PubMed: 7624126]

Frank AJ, Hernan R, Hollander A, Lindsey JC, Lusher ME, Fuller CE, Clifford SC, Gilbertson RJ. The TP53-ARF tumor suppressor pathway is frequently disrupted in large/cell anaplastic medulloblastoma. Brain Res Mol Brain Res. 2004; 121:137–140. [PubMed: 14969745]

Gentles AJ, Alizadeh AA, Lee SI, Myklebust JH, Shachaf CM, Shahbaba B, Levy R, Koller D, Plevritis SK. A pluripotency signature predicts histologic transformation and influences survival in follicular lymphoma patients. Blood. 2009; 114:3158–3166. [PubMed: 19636063]

Gibson P, Tong Y, Robinson G, Thompson MC, Currle DS, Eden C, Kranenburg TA, Hogg T, Poppleton H, Martin J, et al. Subtypes of medulloblastoma have distinct developmental origins. Nature. 2010; 468:1095–1099. [PubMed: 21150899]

Gilbertson RJ, Ellison DW. The origins of medulloblastoma subtypes. Annu Rev Pathol. 2008; 3:341–365. [PubMed: 18039127]

Grotzer MA, Hogarty MD, Janss AJ, Liu X, Zhao H, Eggert A, Sutton LN, Rorke LB, Brodeur GM, Phillips PC. MYC messenger RNA expression predicts survival outcome in childhood primitive neuroectodermal tumor/medulloblastoma. Clin Cancer Res. 2001; 7:2425–2433. [PubMed: 11489822]

Hanel W, Moll UM. Links between mutant p53 and genomic instability. J Cell Biochem. 2011

Harrington EA, Bennett MR, Fanidi A, Evan GI. c-Myc-induced apoptosis in fibroblasts is inhibited by specific cytokines. EMBO J. 1994; 13:3286–3295. [PubMed: 8045259]

Hartmann W, Digon-Sontgerath B, Koch A, Waha A, Endl E, Dani I, Denkhaus D, Goodyer CG, Sorensen N, Wiestler OD, Pietsch T. Phosphatidylinositol 3′-kinase/AKT signaling is activated in medulloblastoma cell proliferation and is associated with reduced expression of PTEN. Clin Cancer Res. 2006; 12:3019–3027. [PubMed: 16707597]

Hemann MT, Bric A, Teruya-Feldstein J, Herbst A, Nilsson JA, Cordon-Cardo C, Cleveland JL, Tansey WP, Lowe SW. Evasion of the p53 tumour surveillance network by tumour-derived MYC mutants. Nature. 2005; 436:807–811. [PubMed: 16094360]

Hermeking H, Eick D. Mediation of c-Myc-induced apoptosis by p53. Science. 1994; 265:2091–2093. [PubMed: 8091232]

Hoshida Y, Brunet JP, Tamayo P, Golub TR, Mesirov JP. Subclass mapping: identifying common subtypes in independent disease data sets. PLoS One. 2007; 2:e1195. [PubMed: 18030330]

Huang MJ, Cheng YC, Liu CR, Lin S, Liu HE. A small-molecule c-Myc inhibitor, 10058-F4, induces cell-cycle arrest, apoptosis, and myeloid differentiation of human acute myeloid leukemia. Exp Hematol. 2006; 34:1480–1489. [PubMed: 17046567]

Jain M, Arvanitis C, Chu K, Dewey W, Leonhardt E, Trinh M, Sundberg CD, Bishop JM, Felsher DW. Sustained loss of a neoplastic phenotype by brief inactivation of MYC. Science. 2002; 297:102–104. [PubMed: 12098700]

Kawamura T, Suzuki J, Wang YV, Menendez S, Morera LB, Raya A, Wahl GM, Belmonte JC. Linking the p53 tumour suppressor pathway to somatic cell reprogramming. Nature. 2009; 460:1140–1144. [PubMed: 19668186]

Kim J, Woo AJ, Chu J, Snow JW, Fujiwara Y, Kim CG, Cantor AB, Orkin SH. A Myc network accounts for similarities between embryonic stem and cancer cell transcription programs. Cell. 2010; 143:313–324. [PubMed: 20946988]

Kool M, Koster J, Bunt J, Hasselt NE, Lakeman A, van Sluis P, Troost D, Meeteren NS, Caron HN, Cloos J, et al. Integrated genomics identifies five medulloblastoma subtypes with distinct genetic profiles, pathway signatures and clinicopathological features. PLoS ONE. 2008; 3:e3088. [PubMed: 18769486]

Kumar A, Marques M, Carrera AC. Phosphoinositide 3-kinase activation in late G1 is required for c-Myc stabilization and S phase entry. Mol Cell Biol. 2006; 26:9116–9125. [PubMed: 17015466]

Kupershmidt I, Su QJ, Grewal A, Sundaresh S, Halperin I, Flynn J, Shekar M, Wang H, Park J, Cui W, et al. Ontology-based meta-analysis of global collections of high-throughput public data. PLoS One. 2010; 5

Lamb J, Crawford ED, Peck D, Modell JW, Blat IC, Wrobel MJ, Lerner J, Brunet JP, Subramanian A, Ross KN, et al. The Connectivity Map: using gene-expression signatures to connect small molecules, genes, and disease. Science. 2006; 313:1929–1935. [PubMed: 17008526]

Lee A, Kessler JD, Read TA, Kaiser C, Corbeil D, Huttner WB, Johnson JE, Wechsler-Reya RJ. Isolation of neural stem cells from the postnatal cerebellum. Nat Neurosci. 2005; 8:723–729. [PubMed: 15908947]

Leonard JR, Cai DX, Rivet DJ, Kaufman BA, Park TS, Levy BK, Perry A. Large cell/anaplastic medulloblastomas and medullomyoblastomas: clinicopathological and genetic features. J Neurosurg. 2001; 95:82–88. [PubMed: 11453402]

Lumpkin EA, Collisson T, Parab P, Omer-Abdalla A, Haeberle H, Chen P, Doetzlhofer A, White P, Groves A, Segil N, Johnson JE. Math1-driven GFP expression in the developing nervous system of transgenic mice. Gene Expr Patterns. 2003; 3:389–395. [PubMed: 12915300]

Meerbrey KL, Hu G, Kessler JD, Roarty K, Li MZ, Fang JE, Herschkowitz JI, Burrows AE, Ciccia A, Sun T, et al. The pINDUCER lentiviral toolkit for inducible RNA interference in vitro and in vivo. Proc Natl Acad Sci U S A. 2011; 108:3665–3670. [PubMed: 21307310]

Meletis K, Wirta V, Hede SM, Nister M, Lundeberg J, Frisen J. p53 suppresses the self-renewal of adult neural stem cells. Development. 2006; 133:363–369. [PubMed: 16368933]

Nagao M, Campbell K, Burns K, Kuan CY, Trumpp A, Nakafuku M. Coordinated control of self-renewal and differentiation of neural stem cells by Myc and the p19ARF-p53 pathway. J Cell Biol. 2008; 183:1243–1257. [PubMed: 19114593]

Northcott PA, Korshunov A, Witt H, Hielscher T, Eberhart CG, Mack S, Bouffet E, Clifford SC, Hawkins CE, French P, et al. Medulloblastoma Comprises Four Distinct Molecular Variants. J Clin Oncol. 2010 In press.

Palmer SL, Reddick WE, Gajjar A. Understanding the Cognitive Impact on Children Who Are Treated for Medulloblastoma. J Pediatr Psychol. 2007

Pelengaris S, Rudolph B, Littlewood T. Action of Myc in vivo - proliferation and apoptosis. Curr Opin Genet Dev. 2000; 10:100–105. [PubMed: 10679391]

Pfister S, Remke M, Benner A, Mendrzyk F, Toedt G, Felsberg J, Wittmann A, Devens F, Gerber NU, Joos S, et al. Outcome prediction in pediatric medulloblastoma based on DNA copy-number aberrations of chromosomes 6q and 17q and the MYC and MYCN loci. J Clin Oncol. 2009; 27:1627–1636. [PubMed: 19255330]

Polkinghorn WR, Tarbell NJ. Medulloblastoma: tumorigenesis, current clinical paradigm, and efforts to improve risk stratification. Nat Clin Pract Oncol. 2007; 4:295–304. [PubMed: 17464337]

Remke M, Hielscher T, Northcott PA, Witt H, Ryzhova M, Wittmann A, Benner A, von Deimling A, Scheurlen W, Perry A, et al. Adult Medulloblastoma Comprises Three Major Molecular Variants. J Clin Oncol. 2011

Schuller U, Heine VM, Mao J, Kho AT, Dillon AK, Han YG, Huillard E, Sun T, Ligon AH, Qian Y, et al. Acquisition of granule neuron precursor identity is a critical determinant of progenitor cell competence to form Shh-induced medulloblastoma. Cancer Cell. 2008; 14:123–134. [PubMed: 18691547]

Shakhova O, Leung C, van Montfort E, Berns A, Marino S. Lack of Rb and p53 delays cerebellar development and predisposes to large cell anaplastic medulloblastoma through amplification of N-Myc and Ptch2. Cancer Res. 2006; 66:5190–5200. [PubMed: 16707443]

Soucek L, Whitfield J, Martins CP, Finch AJ, Murphy DJ, Sodir NM, Karnezis AN, Swigart LB, Nasi S, Evan GI. Modelling Myc inhibition as a cancer therapy. Nature. 2008; 455:679–683. [PubMed: 18716624]

Stavrou T, Bromley CM, Nicholson HS, Byrne J, Packer RJ, Goldstein AM, Reaman GH. Prognostic factors and secondary malignancies in childhood medulloblastoma. J Pediatr Hematol Oncol. 2001; 23:431–436. [PubMed: 11878577]

Stearns D, Chaudhry A, Abel TW, Burger PC, Dang CV, Eberhart CG. c-myc overexpression causes anaplasia in medulloblastoma. Cancer Res. 2006; 66:673–681. [PubMed: 16423996]

Subramanian A, Tamayo P, Mootha VK, Mukherjee S, Ebert BL, Gillette MA, Paulovich A, Pomeroy SL, Golub TR, Lander ES, Mesirov JP. Gene set enrichment analysis: a knowledge-based approach for interpreting genome-wide expression profiles. Proc Natl Acad Sci U S A. 2005; 102:15545–15550. [PubMed: 16199517]

Sutter R, Shakhova O, Bhagat H, Behesti H, Sutter C, Penkar S, Santuccione A, Bernays R, Heppner FL, Schuller U, et al. Cerebellar stem cells act as medulloblastoma-initiating cells in a mouse model and a neural stem cell signature characterizes a subset of human medulloblastomas. Oncogene. 2010; 29:1845–1856. [PubMed: 20062081]

Swartling FJ, Grimmer MR, Hackett CS, Northcott PA, Fan QW, Goldenberg DD, Lau J, Masic S, Nguyen K, Yakovenko S, et al. Pleiotropic role for MYCN in medulloblastoma. Genes Dev. 2010; 24:1059–1072. [PubMed: 20478998]

Tabori U, Baskin B, Shago M, Alon N, Taylor MD, Ray PN, Bouffet E, Malkin D, Hawkins C. Universal poor survival in children with medulloblastoma harboring somatic TP53 mutations. J Clin Oncol. 2010; 28:1345–1350. [PubMed: 20142599]

Thompson MC, Fuller C, Hogg TL, Dalton J, Finkelstein D, Lau CC, Chintagumpala M, Adesina A, Ashley DM, Kellie SJ, et al. Genomics identifies medulloblastoma subgroups that are enriched for specific genetic alterations. J Clin Oncol. 2006; 24:1924–1931. [PubMed: 16567768]

Wang J, Wang H, Li Z, Wu Q, Lathia JD, McLendon RE, Hjelmeland AB, Rich JN. c-Myc is required for maintenance of glioma cancer stem cells. PLoS ONE. 2008; 3:e3769. [PubMed: 19020659]

Yang ZJ, Ellis T, Markant SL, Read TA, Kessler JD, Bourboulas M, Schuller U, Machold R, Fishell G, Rowitch DH, et al. Medulloblastoma can be initiated by deletion of Patched in lineage-restricted progenitors or stem cells. Cancer Cell. 2008; 14:135–145. [PubMed: 18691548]

Zheng H, Ying H, Yan H, Kimmelman AC, Hiller DJ, Chen AJ, Perry SR, Tonon G, Chu GC, Ding Z, et al. p53 and Pten control neural and glioma stem/progenitor cell renewal and differentiation. Nature. 2008; 455:1129–1133. [PubMed: 18948956]

Zhu J, Blenis J, Yuan J. Activation of PI3K/Akt and MAPK pathways regulates Myc-mediated transcription by phosphorylating and promoting the degradation of Mad1. Proc Natl Acad Sci U S A. 2008; 105:6584–6589. [PubMed: 18451027]

SIGNIFICANCE

Animal models are valuable for studying the origins and molecular mechanisms of cancer, and can be used to develop and test new therapeutic strategies. Existing mouse models of MB have been extremely useful for studying MB associated with Sonic Hedgehog (SHH) pathway mutations. In contrast, no models have been developed to study MYC-driven MB. Here we describe a mouse model of this tumor based on transplantation of cerebellar stem cells expressing *Myc* and dominant-negative *p53* (*DNp53*). These tumors resemble human MYC-driven MB at a histological and molecular level, and can be inhibited by antagonists of the PI3K/mTOR pathway. This model represents an important new tool for studying the biology and therapeutic responsiveness of MYC-driven MB.

HIGHLIGHTS

- *Myc* promotes proliferation of cerebellar stem cells *in vitro*
- Mutant *p* cooperates with *53 Myc* to transform stem cells into tumors
- Tumors resulting from *Myc* and mutant *p53* resemble human MYC-driven MB
- Tumors are inhibited by PI3K/mTOR antagonists

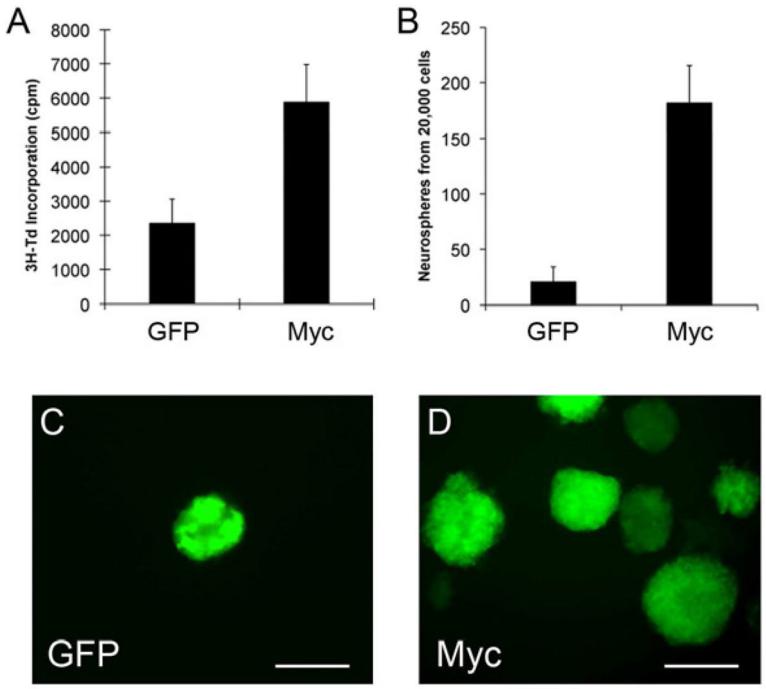

Figure 1. *Myc* promotes proliferation of cerebellar stem cells *in vitro*

(A), Prom1^{+}Lin^{-} cells sorted from cerebella of 5–7 day-old mice were infected with *Myc*-IRES-GFP or control (GFP only) viruses for 48h, pulsed with tritiated thymidine (^{3}H-Td) and cultured overnight before being assayed for ^{3}H-Td incorporation. Data represent means of triplicate samples ± SEM. (B–D) Prom1^{+}Lin^{-} cells infected with *Myc*-IRES-GFP or control viruses were cultured at low density in the presence of EGF and bFGF for 7 days. Representative fields are shown in panels C and D (scale bars = 100 μm). The number of GFP^{+} neurospheres is quantified in B; data represent means of triplicate samples ± SEM. The infection efficiency was 80% with *Myc*-IRES-GFP and 90% with control retrovirus. See also Figure S1.

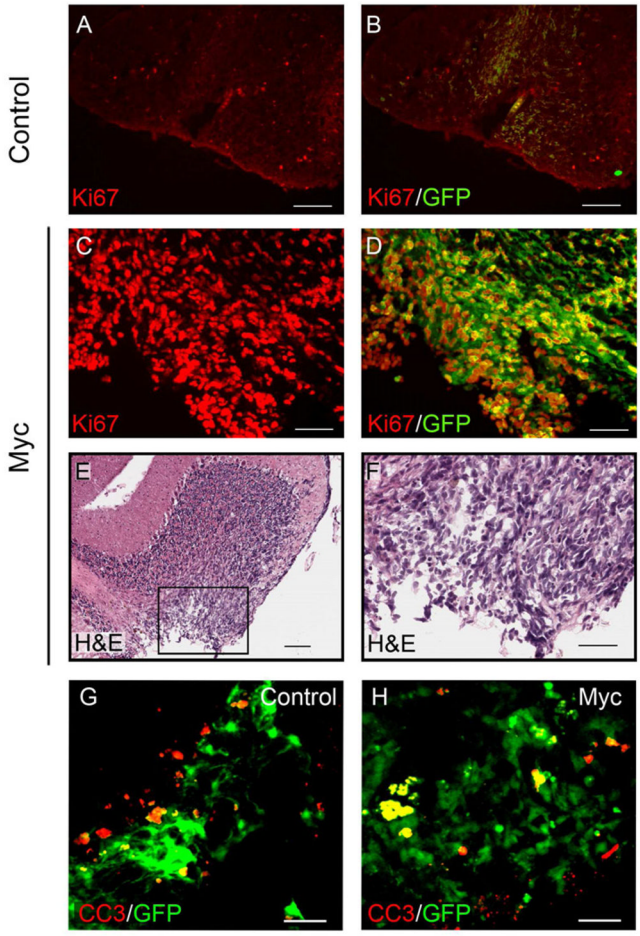

Figure 2. *Myc*-infected stem cells give rise to transient hyperplastic lesions following transplantation

Prom1^{+}Lin^{-} cells were infected with *Myc*-IRES-GFP or control retroviruss for 20h and then transplanted into the cerebellum of NSG mice. Hosts were sacrificed after 2.5 weeks. Frozen sections from mice that received GFP-infected (A–B) or *Myc* infected cells (C–F) were stained with anti-Ki67 antibodies (A–D) or H&E (E, F). Note the large mass of proliferating (Ki67^{+}) cells seen in animals that received *Myc*-infected cells (C, D). Box in E corresponds to high-power field shown in F. Panels A–D and F, scale bars = 50 μm; panel E, scale bar = 100 μm. (G–H) Prom1^{+} cells were infected with *Myc*-ires-GFP or control-GFP viruses for 20h and then transplanted into the cerebellum of NSG hosts. Mice were sacrificed after 2 weeks. Frozen sections from mice that received control (G) or *Myc* infected cells (H) were stained with antibodies specific for cleaved caspase-3 (CC3) to detect apoptotic cells. Scale bars = 50 μm. See also Figure S2.

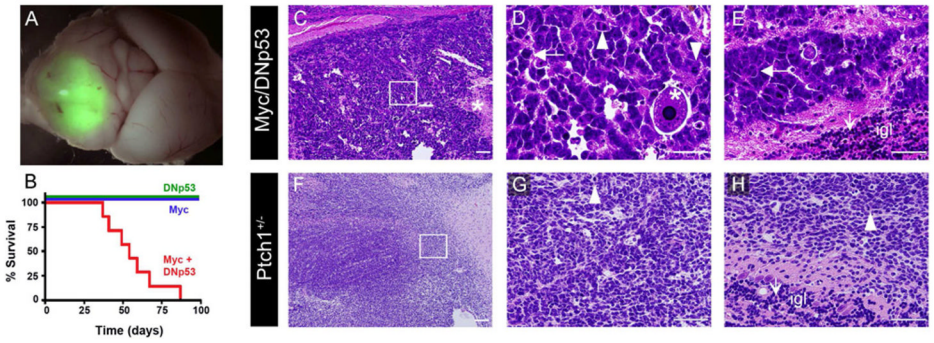

Figure 3. Overexpression of *Myc* and inactivation of *p53* transforms cerebellar stem cells into tumors

Prom1^{+}Lin^{-} cells were infected with *Myc* + *DNp53* retroviruses, *Myc* alone or *DNp53* alone for 20h, and transplanted into cerebella of NSG mice. Animals were sacrificed when they developed symptoms. (A), Whole mount image of tumor, with GFP expression originating from *DNp53* retrovirus. (B) Survival curve of animals receiving 5 x10^{4} cells infected with *Myc* viruses (blue line), *DNp53* viruses (green line) or *Myc* + *DNp53* viruses (red line) (median survival 48 days). (C–H) Sections of tumor tissue from animals transplanted with cells expressing *Myc* and *DNp53* (C–E) or from *Ptch1* mutant mice (F–H) were stained with hematoxylin and eosin. For C and F scale bars = 100 μm; for D, E, G and H, scale bars = 50 μm. Boxes in panels C and F refer to panels D and G, respectively. Asterisk in C shows an area of necrosis, and asterisk in D shows a large tumor cell with marked nuclear atypia (anaplasia). Horizontal arrows in D and E show prominent nuclear molding. Arrowheads in D, G and H show mitotic figures. Vertical arrows in E and H show normal granule neurons in the internal granule layer (igl); the majority of tumor cells in E are much larger than these cells, whereas those in H are approximately the same size. See also Figure S3.

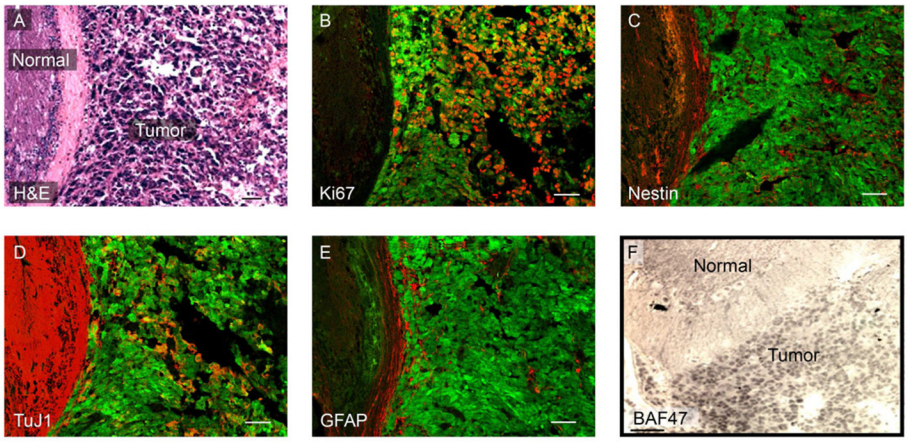

Figure 4. MP tumors exhibit characteristics of human MB

Cryosections from MP tumors were stained with H&E (A) or with antibodies specific for Ki67 (B), Nestin (C), Tuj1 (D), GFAP (E) or BAF47/Ini1 (F). Panels A–E represent adjacent sections. Scale bars = 50 μm. See also Figure S4.

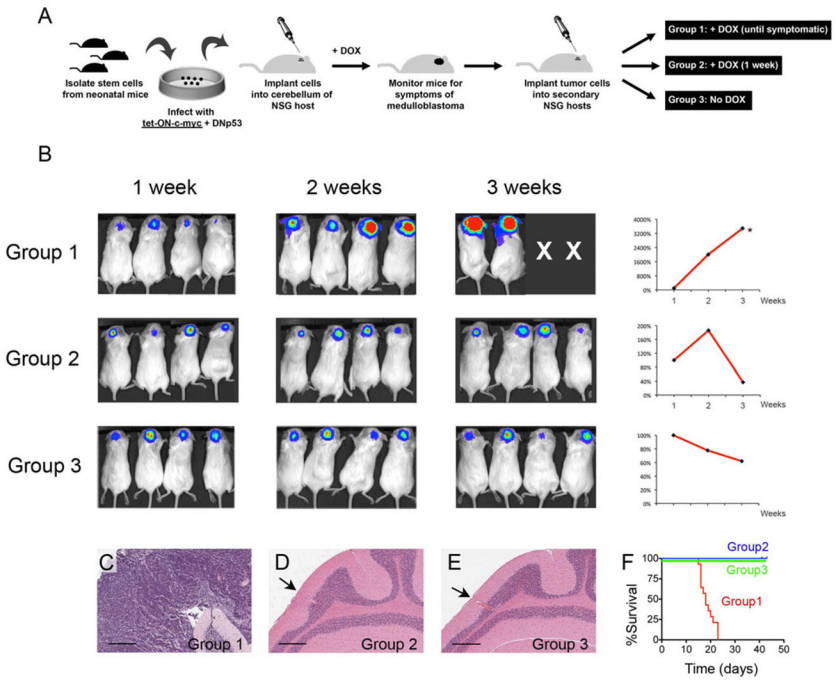

Figure 5. ***Myc*** **is required for continued growth of MP tumors**

(A) Strategy for generating Tet-regulatable MP tumors. (B–F) Bioluminescent imaging of animals at 1, 2 and 3 weeks after tumor cells transplantation. Panel B shows representative images of 4 animals from each group at each time point (X's denote animals that died before they could be imaged). Graphs on right show mean percent increase in bioluminescence for all animals in the group (with the 1-week signal for each animal set at 100%). In the top graph, the 1- and 2-week time points represent the average signal intensity for all 14 animals; the 3-week time point (marked by asterisk) represents the average for the 3 animals that remained alive at the time of imaging. (C–E) H&E-stained cerebellar sections from representative animals in Groups 1 (C), 2 (D) and 3 (E) three weeks after transplantation. Arrows in D and E point to injection site. Scale bars = 250 μm. (F) Survival curve (Groups 1 and 2, n=14; Group 3, n=12).

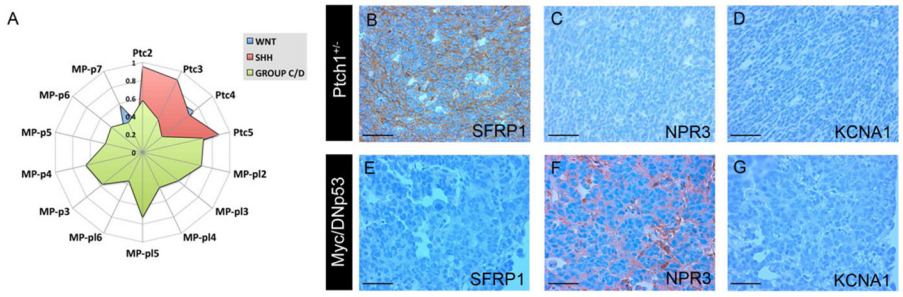

Figure 6. MP tumors resemble human MYC-driven MB

A, Gene expression profiles of *Myc*/*DNp53* tumors from Prom1^{+}/Lin^{-} cells (MP-pl2-6) or from Prom1^{+} cells (MP-P3-7) and *Ptch1* mutant (Ptc1-4) tumors were compared to signatures generated from human MB subtypes: WNT (blue), SHH (red), and Group C/D (green). Each murine tumor was assigned a score denoting its similarity to each subtype of human tumor (for details see Human Tumor Analysis Supplement and Table S1). (B–G) *Ptch1* and MP tumors were stained with antibodies specific for secreted frizzled-related protein 1 (SFRP1, a marker for SHH tumors), Natriuretic Peptide Receptor C (NPR3, a marker for Group C tumors), or Potassium voltage-gated channel, shaker-related subfamily, member 1 (KCNA1, a marker for Group D tumors). Scale bars = 100 μm. See also Figure S5 and Table S1.

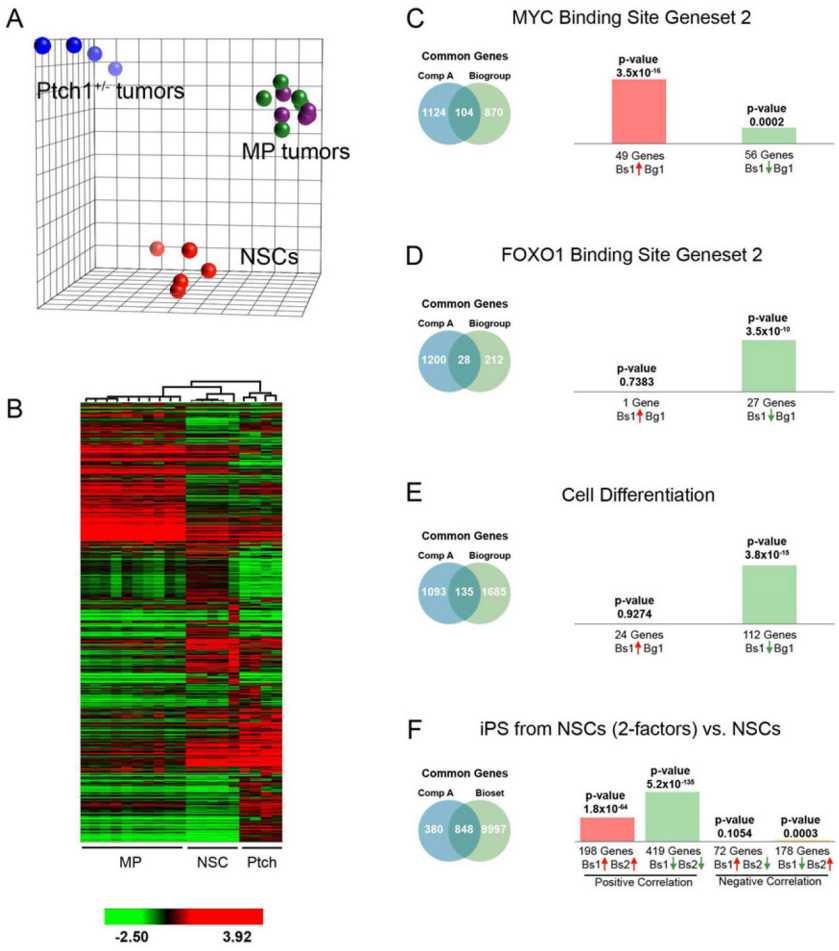

Figure 7. MP tumors are molecularly distinct from stem cells and from *Ptch1* tumors

(A) Principle components analysis (PCA). Three PCA coordinates describe 55.2% of total data variation (PC1 – 27.2%, PC2 – 19.8% and PC3 – 8.23%). Green, MP tumors derived from Prom1^{+}Lin^{-} cells; purple, MP tumors derived from Prom1^{+} cells; blue, *Ptch1* tumors; red, normal stem cells (NSCs). (B) Unsupervised hierarchical clustering analysis. Each column represents a distinct sample and each row represents an individual gene. The normalized (log2) and standardized (each sample to mean signal = 0 and standard deviation = 1) level of gene expression is denoted by color (green = low, dark = intermediate, red = high) as indicated in the gradient at the bottom. (C–F) Genes differentially expressed between MP tumors and *Ptch1* tumors were subjected to NextBio analysis, to identify Biogroups and Studies that contain similar genes. Representative Biogroups (C–D, E) and Studies (F) are shown. Venn diagrams show the number of common and unique genes in both sets. Bars on the right show the significance of overlap between gene subsets (the scale of the bar is measured in −log(p-value), so taller the bar, the higher the significance of the gene overlap). Whereas each Biogroup is represented by a single list of genes, signature genes from Studies have two lists, one for up-regulated and one for down-regulated genes. Thus, Biogroup comparisons consist of just two graphs, whereas comparisons to Studies consist of four graphs. See also Tables S2–6.

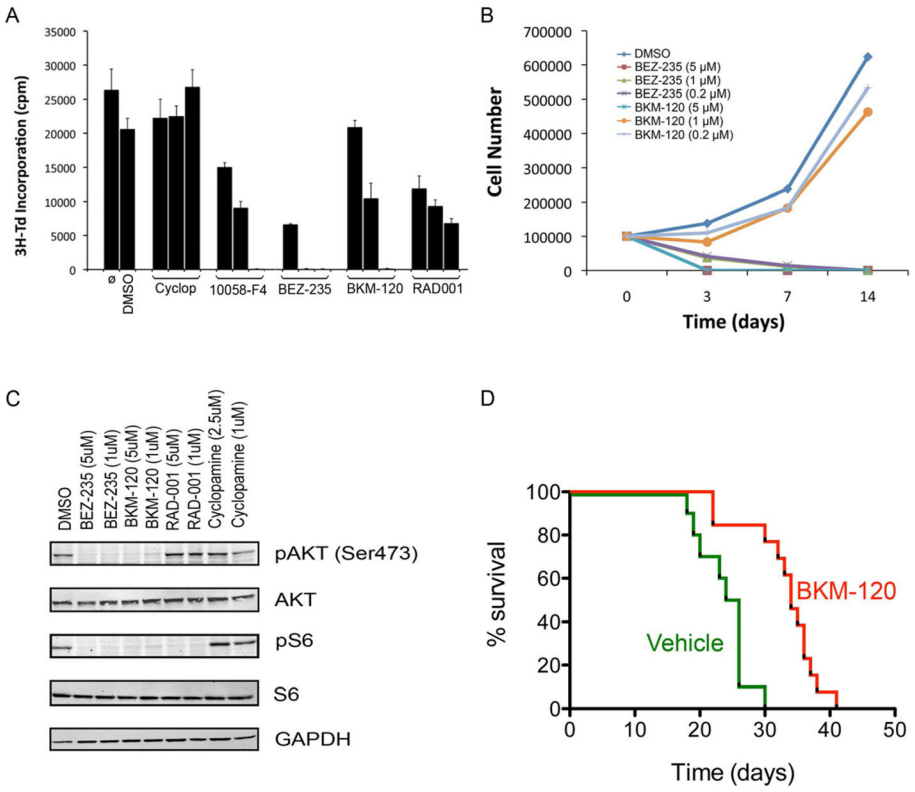

Figure 8. Growth of MP tumor cells is inhibited by antagonists of PI3K/mTOR signaling

(A) Effects of inhibitors on short-term proliferation. MP tumor cells were cultured in serum-free media containing no additive (ø), vehicle (DMSO), cyclopamine (0.1, 1, 2.5 μM), 10058-F4 (10, 25, 100 μM), BEZ-235 (0.2, 1, 5 μM), BKM-120 (0.2, 1, 5μM), or RAD-001 (0.2, 1, 5μM). For each inhibitor, columns are ordered from lowest to highest concentration. After 48h, cells were pulsed with ^{3}H-Td and cultured overnight before being assayed for ^{3}H-Td incorporation. Data represent means of triplicate samples ± SEM. (B) Effects on long-term growth. Tumor cells were cultured for 3, 7 or 14 days in the presence of different doses of inhibitors and cell number was counted at the indicated time points. (C) Effects on PI3K signaling. Tumor cells were treated with DMSO, BEZ-235 (5uM, 1uM), BKM-120 (5uM, 1uM), RAD-001(5uM, 1uM) or cyclopamine (2.5uM, 1uM) for 3 hr. Cells were lysed and protein was analyzed for phosphorylation of AKT and S6 (pAKT and pS6) or for GAPDH by Western blotting. (D) Effects on tumor growth in vivo. 500 MP tumor cells were re-transplanted into naïve NSG mice. After 7 days, mice were imaged for luciferase activity and separated into two groups randomly. Mice in Group 1 were treated with vehicle (0.5% methyl-cellulose) and those in Group 2 were treated with BKM-120 (30mg/kg per day) by oral gavage until they developed symptoms. BMK-120 treatment significantly prolonged survival compared to vehicle (p=0.001). See also Figure S6.